Tellus (2007), 59A, 182–197
Printed in Singapore. All rights reserved

TELLUS

Interpretation of discrete and continuum modes in a two-layer Eady model

By HYLKE DE VRIES* and THEO OPSTEEGH, *Institute for Marine and Atmospheric Research Utrecht, Princetonplein 5, 3584CC, Utrecht, Netherlands*

(Manuscript received 8 June 2006; in final form 25 October 2006)

ABSTRACT

The upper rigid lid of the conventional Eady model for baroclinic instability is replaced by a more realistic stratosphere with an increased buoyancy frequency and a different shear of the zonal wind. Previously reported results of a normal-mode stability analysis are re-interpreted using the concept of interacting surface and tropopause PV anomalies, called PV building blocks (PVBs). In this perspective, which directly relates to the counter-propagating Rossby wave formalism, the appearance of both the short-wave and the long-wave cut-off becomes physically transparent.

New results include a discussion of the continuum modes in terms of interacting PVBs. Continuum modes are modal solutions to the inviscid linearised equations, specified by non-zero PV at one interior level (as well as non-zero PV at the surface and the tropopause). If the stratospheric zonal wind decreases with height, the continuum modes cause resonances at multiple (even stratospheric) levels. These resonant continuum modes may play an important role in the explanation of disturbance growth from initial conditions in which the discrete normal modes are neutral.

1. Introduction

It needs no introduction that the linear stability of the Eady (1949) model depends completely on the formulation of the boundary conditions. In its original formulation, rigid lids are prescribed at two levels in the vertical which represent the Earth surface and the level of the tropopause. Potential temperature (PT) anomalies propagate along these rigid lids. If the conditions are favourable, instability sets in as a sustained interaction between the surface and the tropopause PT anomalies, a classic result to be found in any textbook (see e.g. Pedlosky, 1987). On the other hand, if the rigid lid approximation is not made at the level of the tropopause, but one assumes that the perturbation vanishes at infinite height, exponential instability does not occur because there is no upper-level edge wave.

This paper discusses an alternative to both above-mentioned descriptions and replaces the upper rigid lid by an unbounded stratosphere-like domain. For the troposphere the effect of replacing the rigid lid by a stratosphere is to replace the rigid top boundary by a top boundary which is essentially a free one. The troposphere is specified by a constant buoyancy frequency N^2 and a constant vertical shear Λ of the zonal wind $\bar{u}$, such that the basic-state PV is uniform if one neglects the meridional dependence of the Coriolis parameter. The shear and buoyancy frequency attain different values in the stratosphere.

Replacing the upper rigid lid by a second, vertically unbounded layer with uniform PV is not a novel approach. Müller (1991) investigated the normal-mode stability properties of such a two-layer Eady model, showing the existence of growing normal modes of intermediate wavenumbers, i.e. both a long-wave and a short-wave cut-off exist. On the short-wave neutral branch, the neutral modes are confined to either the surface or the tropopause. Furthermore, Müller (1991) argues that the long-wave neutral normal modes are related to either the lower or the upper layer. The reasoning is based on an asymptotic expansion in the wavenumber of the dispersion relation, an approach which makes it difficult to understand the results physically.

The present paper offers an alternative to Müller's interpretation of the normal-mode results by systematically interpreting them in the more physically intuitive view of interacting PV anomalies, or counter-propagating Rossby waves (CRW) as formulated for instance by Hoskins et al. (1985) and Heifetz et al. (2004a). Although Müller (1991) makes the connection with the PV perspective, a systematic treatment of the problem is not presented. The existence of long-wave neutral modes, which are absent in the classic Eady model, becomes physically transparent adopting the PV view. Furthermore, we will show that the absence of a long-wave cut-off should be considered as an exception rather than the rule.

Let us briefly summarise other studies of two-layer variants of the Eady model. Rivest et al. (1992) investigated in more detail

*Corresponding author. Current affiliation: Department of Meteorology, University of Reading, Reading, UK
e-mail: hdv.atmos@gmail.com
DOI: 10.1111/j.1600-0870.2006.00219.x

the case of zero shear of the stratospheric zonal wind, showing that both the growth rate and the wavenumber of the most rapidly growing wave decrease compared to the classic rigid lid case. Juckes (1994) analysed the dynamics of PT anomalies at the tropopause, showing that the tropopause becomes undulated in the presence of perturbations as a result of continuity requirements.

Prior to Müller (1991), Blumen (1979) and Weng and Barcilon (1987) had already investigated two-layer Eady models which are bounded from above by a second rigid lid. Those models sustain short-wave unstable modes. Further back in time, Simmons (1974) had investigated baroclinic instability occurring in a model of the stratopause (a vertically unbounded westerly sheared flow with a buoyancy frequency decrease across the stratopause). He used the β-plane approximation to ensure the fulfilment of the Charney-Stern criterion. A more advanced study is the work of Song and Nakamura (2000) who treat a two-layer semi-geostrophic variant of the Eady model numerically for a highly complex basic state with an isolated jet and a meridionally varying tropopause height. Recently, Bordi et al. (2002) discussed the two-layer Eady model in the context of a possible neutralisation theory of climate.

Non-linear stability of the Eady model has first been investigated by Mu and Shepherd (1994), thereafter optimised by Liu and Mu (1996) and generalised to include β in Liu and Mu (2001). Finally, Ripa (2001) (and references therein) also investigated the non-linear stability of Eady-like models with sloped, rigid, or free boundaries. In contrast to the former authors, who had in mind the application to the atmosphere, the lower layer of Ripa (2001) is motionless and unbounded from below (and simulates the deep ocean) and the upper layer has non-zero vertical shear. Moreover, Ripa (2001) does not include the jump of the buoyancy frequency at the layer interface, which is an essential property of the atmosphere.

One element the above-mentioned papers have in common is that none of them tries to interpret and explain the normal-mode results in terms of the PV perspective. As mentioned previously, the present paper aims to fill in that gap. But in this field important steps have been undertaken as well.

The classic interpretation of Eady-type baroclinic instability dates back to Bretherton (1966). Heifetz et al. (2004a) generalised the CRW-perspective and interpreted the evolution of unstable discrete normal modes in terms of interacting CRWs for much more general flow. These CRWs can be constructed in two qualitatively different ways, which both find their origin in the edge-wave interpretation of the Eady model as discussed in Davies and Bishop (1994). The way to derive expressions for the CRWs which stay closest to PV thinking of Hoskins et al. (1985) is the so-called home-base method and the PVBs used in the present paper are in fact identical to the CRWs constructed using the home-base method. We will adopt the term PVB, since the CRW has been generalised recently far beyond its traditional, Eady-like form (Heifetz et al., 2004a,b; Methven et al., 2005a,b). Last mentioned studies allow the understanding of baroclinic instability for much more complex dynamics and basic states. However, whereas their focus is mainly on growing normal modes, the present paper attacks a much simpler setting but extends the previous papers in the sense that we pay specific attention to the neutral discrete NMs as well as to an interpretation of the continuous spectrum. Both topics have been left largely in-discussed in the above-mentioned papers.

2. Model and basic flow

2.1. Dynamics

We consider linear quasi-geostrophic dynamics on an f-plane. The domain is divided in two layers of uniform (but different) quasi-geostrophic potential vorticity (PV). The lower layer, which is in direct contact with the surface, is the troposphere. The upper layer, which is unbounded from above, is the stratosphere. The interface between the layer is the tropopause, which is kept at a reference height d. The shear Λ of the zonal wind $\bar{u}$ and the buoyancy frequency N^2 of the troposphere and the stratosphere are specified separately.

Throughout this paper the subscript $i = (s, t)$ added to perturbation or basic-state quantities indicates the stratospheric or tropospheric part of that quantity respectively. We will therefore not use the t in subscript to indicate partial derivative with respect to time. Furthermore, basic-state quantities will be denoted by an over bar.

The dynamics of the perturbations evolving on the basic state [specified by $\bar{u}_i(z)$ and $N_i^2(z)$] is governed by material conservation of PV q_i in each layer

$$\frac{\mathrm{Dq}_i}{\mathrm{Dt}} = 0, \quad q_i = \left[\frac{\partial^2}{\partial x^2} + \frac{\partial^2}{\partial y^2} + \frac{\partial}{\partial z}\left(\frac{1}{N_i^2}\frac{\partial}{\partial z}\right)\right]\psi_i \tag{1}$$

where $\mathrm{D}/\mathrm{D}t = \partial/\partial t + \bar{u}_i\partial/\partial x$ and ψ_i the stream-function in layer i. Variables have been made non-dimensional using standard scalings ($L = 1000$ km, $H = 10$ km, $U = 30$ m s^{-1}), (Pedlosky, 1987). Given these scalings, the Burger number $B \equiv (N_0^2 H^2 f_0^{-2} L^{-2}) = 1$ and the Rossby number $Ro \equiv f_0^{-1} U L^{-1} = 0.3$.

2.2. Basic state

The basic state has both a continuous wind profile and a continuous potential temperature structure. Such continuity requirements inevitably lead to a meridionally sloped tropopause height $z_{\mathrm{tp}}(y)$:

$$z_{\mathrm{tp}} = d - \sigma y, \quad \sigma = \left(\frac{\Lambda_t - \Lambda_s}{N_s^2 - N_t^2}\right) Ro. \tag{2}$$

Realistic basic states ($N_s^2 \geq N_t^2$ and $\Lambda_s \leq \Lambda_t$) will therefore have a tropopause height which decreases pole-ward. The tropopause slope σ is zero only if $\Lambda_t = \Lambda_s$. Eq. (2) also implies that a

continuous basic state cannot be obtained if $N_s^2 = N_t^2$ but $\Lambda_s \neq \Lambda_t$. Phrased differently, if the zonal wind has its maximum at the tropopause level, a change in basic-state buoyancy frequency is required to guarantee a continuous basic state.

2.3. Boundary and interface conditions

Boundary conditions at the surface and the top of the atmosphere as well as a proper interface condition are required to determine the stream-function $\psi_{s,t}$ of perturbations of the basic state. The condition that the vertical velocity w equals zero at the surface (rigid lid condition) leads to

$$\frac{\mathrm{D}\theta}{\mathrm{Dt}} + v\frac{\partial\bar{\theta}}{\partial y} = -wN^2 = 0 \quad (z = 0) \tag{3}$$

where $\theta \equiv \partial\psi/\partial z$, the non-dimensional potential temperature (PT) and $v = \partial\psi/\partial x$, the meridional velocity. At the top of the atmosphere ($z \to \infty$) we require vanishing ψ.

The interface condition is prescribed as the requirement that both the stream-function and the velocity normal to the (sloping) tropopause are continuous across the tropopause. Using the smallness of σ in terms of Ro [eq. (2)], one gets (Rivest et al., 1992):

$$w_t - \boldsymbol{u}_t \cdot \nabla z_{\mathrm{tp}} = w_s - \boldsymbol{u}_s \cdot \nabla z_{\mathrm{tp}} + O(Ro^2), \quad [z = z_{\mathrm{tp}}(y)] \tag{4}$$

where $\boldsymbol{u}_i = (u_i, v_i)$ the horizontal velocity field and w_i the vertical velocity in layer i. Since ψ (and therefore u) is continuous at the tropopause, (4) simplifies to $w_t = w_s$ evaluated at $z = z_{\mathrm{tp}}(y)$. In this leading order analysis the evaluation height $z = z_{\mathrm{tp}}(y)$ in (4) can be replaced by $z = d$, similar to discussions involving small bottom topography (Blumsack and Gierasch, 1972; Pedlosky, 1987). Condition (4) then becomes

$$\frac{1}{N_t^2}\left[\left(\frac{\partial}{\partial t} + \bar{u}\frac{\partial}{\partial x}\right)\frac{\partial\psi}{\partial z} - \Lambda_t\frac{\partial\psi}{\partial x}\right]_{z=d-} = \frac{1}{N_s^2}\left[\left(\frac{\partial}{\partial t} + \bar{u}\frac{\partial}{\partial x}\right)\frac{\partial\psi}{\partial z} - \Lambda_s\frac{\partial\psi}{\partial x}\right]_{z=d+} \tag{5}$$

The Eady problem with upper rigid lid is recovered by letting $N_s \to \infty$.

Condition (5) can be interpreted easily in terms of a PV equation as in the Bretherton (1966) approach. The discontinuities of the vertical wind shear and the buoyancy frequency generate a meridional gradient of the basic-state PV at the level of the tropopause. Perturbations with a continuous stream-function ψ at the tropopause will have a different vertical structure in the upward and downward direction due to the different buoyancy frequency in both domains. As a result the PT transits discontinuously across the tropopause. The jump in PT is interpreted as a PV anomaly at the tropopause:

$$\frac{\mathrm{Dq}}{\mathrm{Dt}} + v\frac{\partial\bar{q}}{\partial y} = 0 \quad (z = d), \tag{6}$$

where q and $\bar{q}$ are the integrated singular contributions to the perturbation and basic-state PV. Of course, the PT discontinuity does not occur in reality. What actually happens is that the tropopause becomes undulated. To ensure continuity of the total (basic-state and perturbation) potential temperature across the tropopause, positive (negative) tropopause PV anomalies will result in a low (high) tropopause (Rivest et al., 1992; Juckes, 1994).

2.4. PV building blocks

If one decides to represent the tropopause by a rigid lid, the stream-function is usually decomposed in terms of surface and top PT anomalies which have zero PT at the opposite boundary (Davies and Bishop, 1994). As discussed above, for the two-layer setup the PT is discontinuous at the tropopause. Therefore it makes more sense to decompose the stream-function in terms of two so-called PV building blocks (PVBs) which each have non-zero PV at either the surface (B) or the tropopause (T), the Bretherton (1966) approach. One writes

$$q_B(z) = \delta(z), \quad q_T(z) = \delta(z - d), \tag{7}$$

where $\delta(z)$ is the Dirac delta function. Each PVB has its own associated stream-function (labelled by the same subscript). The total stream-function is written as $\phi(z) = B\phi_B(z) + T\phi_T(z)$, where $B = \hat{B}e^{i\epsilon_B}$ and $T = \hat{T}e^{i\epsilon_T}$ are complex amplitudes. Appendix A lists the expressions for $\phi_{B,T}$. The structure of the two PVBs (scaled to have unit amplitude at the level of their PV) is displayed in Fig. 1a–b for two different stratifications of the stratosphere. The tropospheric stream-function of the tropopause PVB is not influenced by the stratospheric buoyancy frequency N_s^2. In contrast, the tropospheric stream-function of the surface PVB decreases less rapidly with height for large values of N_s^2 to guarantee that the surface PVB has zero PV at the level of the tropopause (in the limit $N_s^2 \to \infty$, the PT at the tropopause is zero).

3. Linear stability analysis

3.1. Dispersion relation

Normal modes (NMs) are wave-like structures of the form $\psi(\boldsymbol{x}, t) = \phi(z)\exp[ik(x - ct)]\cos ly$, where $c = c_r + ic_i$ denotes the (complex) phase-speed. The meridional wavenumber attains the values $l = (n + \frac{1}{2})\pi/Y$ with $(n = 0, 1, \ldots)$ to satisfy the lateral boundary conditions $v = 0$ at $y = \pm Y$. A two-dimensional problem results if we let $Y \to \infty$.

The following sections will only be considered with NMs with zero perturbation PV in the interior of each layer (i.e. pure Eady waves). A discussion of the continuum modes (modal structures with non-zero PV in the interior) is postponed to Section 6. Imposing the rigid lid condition (3) and the interface condition

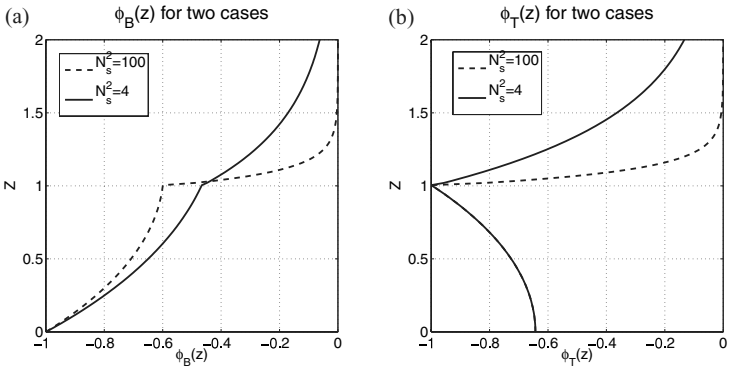

Fig. 1. Stream-function structure of the (a) surface and (b) tropopause PVB with $K = 1$ (scaled to have unit stream-function amplitude at the level of the PV) for two values of N_s^2. The tropopause is located at $z = 1$.

(6) results in

$$\begin{pmatrix} c - c_B & f_B \\ f_T & c - c_T \end{pmatrix} \begin{pmatrix} B \\ T \end{pmatrix} = 0. \tag{8}$$

The diagonal entries c_B and c_T in (8) (Appendix A) define the 'natural' phase-speeds of the surface and tropopause PVB when the other PVB is absent.[1] Please note that pure PVBs are only true solutions to the dynamical equations (i.e. NMs), if both couplings $f_{B,T}$ in (8) are zero. If only one of the coupling terms is zero, the two NMs will still propagate with speeds c_B and c_T, i.e. as if they were a surface PVB or a tropopause PVB, respectively. Their vertical structure, however, will not necessarily (in fact, mostly not at all) be similar to the structure of a pure PVB. The non-trivial solution to (8) gives the NM dispersion relation

$$c = \frac{1}{2}(c_T + c_B) \pm \frac{1}{2}\sqrt{(c_T - c_B)^2 - \Gamma_f}, \quad \Gamma_f = -4 f_B f_T, \tag{9}$$

and Γ_f will be called the 'coupling-function' of the PVBs. Each NM is a complex superposition of the two PVBs. As long as $c_i \neq 0$, the structure of the growing/decaying NM pair is given by[2]

$$\frac{\hat{T}^2}{\hat{B}^2} = -\frac{f_T}{f_B} = \frac{\tilde{\Lambda}_t - \tilde{\Lambda}_s}{\tilde{\Lambda}_t}, \quad \cos(\epsilon_T - \epsilon_B) = \frac{c_B - c_T}{\sqrt{\Gamma_f}} \tag{10}$$

where $\tilde{\Lambda}_t = \Lambda_t N_t^{-2}$ and $\tilde{\Lambda}_s = \Lambda_s N_s^{-2}$ define 'effective' shears of the troposphere and stratosphere. The above relations show that growing and decaying NMs are composed of PVBs with equal amplitudes only if the couplings f_T and f_B are equal and opposite, i.e. if the stratospheric shear is zero. The propagation speed and growth rate of the growing/decaying NM pair are given by

$$c_r = \frac{1}{2}(c_B + c_T), \quad k c_i = \pm\frac{k}{2}\sqrt{\Gamma_f}\sin(\epsilon_T - \epsilon_B). \tag{11}$$

Therefore c_r equals the average of the 'natural' phase speeds of the surface and tropopause PVB.

[1] c_B and c_T are identical to c_1^1 and c_2^2 in Heifetz et al. (2004a), f_B and f_T correspond with c_1^2 and c_2^1.

[2] Please see Heifetz et al. (2004a) for similar results obtained for the general CRW equations [e.g. their equations (48), (53–54)].

If the NMs are neutral ($c_i = 0$), their stream-function satisfies $\sin(\epsilon_T - \epsilon_B) = 0$. To some extent these neutral NMs can be interpreted as modified PVBs (Section 5).

3.2. Resonant wavenumber

In Ripa (2001) the so-called 'resonant' wavenumber K_{res} is defined as the wavenumber at which $c_B = c_T$. By definition, this 'resonant' wavenumber is independent of the couplings $f_{B,T}$. NMs with a wavenumber around this 'resonant' wavenumber will be the first for which the basic state becomes unstable but only if Γ_f is positive [see (9)]. Ripa (2001) showed that this resonant wavenumber does not produce the fastest growing NM.

Müller (1991) discusses a similar 'resonant' wavenumber, based on the equality of the asymptotic short-wave branches of the dispersion relation. Please note that the two wavenumbers are not equal in most cases.

4. Conditions for instability

4.1. Charney-Stern condition: a necessary condition

An examination of the PV distributions sheds more light on the stability characteristics. We write $\bar{q}_y^0$ and $\bar{q}_y^d$ for the mean PV gradients at the surface and the tropopause respectively. A straightforward computation shows that

$$\bar{q}_y^d = \tilde{\Lambda}_t - \tilde{\Lambda}_s, \quad \bar{q}_y^0 = -\tilde{\Lambda}_t. \tag{12}$$

Since the Charney-Stern (1962) condition for instability requires a sign-change in the vertical distribution of PV gradient, marginal stability occurs if

$$\tilde{\Lambda}_s = \tilde{\Lambda}_t \quad \Longleftrightarrow \quad \bar{q}_y^d = 0, \tag{13}$$

while all NMs are neutral for $\tilde{\Lambda}_s > \tilde{\Lambda}_t$ (Müller, 1991).

4.2. Coupling the PVBs: toward a sufficient condition

If the necessary Charney-Stern condition is fulfilled, two additional conditions determine whether instability will actually occur. First, both PVBs should be able to 'sufficiently see'

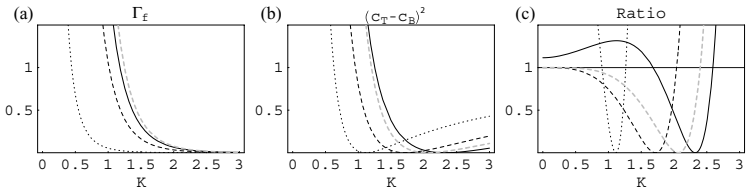

Fig. 2. For $\tilde{\Lambda}_t = 1$, $N_s^2 = 4$ and $\tilde{\Lambda}_s = -0.95$ (full), $\tilde{\Lambda}_s = 0$ (dashed), $\tilde{\Lambda}_s = 0.95$ (dotted) we show as a function of the total horizontal wavenumber K (a) the coupling-term Γ_f of (9), (b) square of the phase-speed difference of the PVBs $(c_T - c_B)^2$, (c) the ratio $(c_T - c_B)^2/\Gamma_f$. The results for the Eady model with upper rigid lid, are displayed by the gray lines.

each other. This includes the well-known Rossby-height effect. Mathematically, the 'see'-criterion is expressed in the coupling-function Γ_f [see (9)]. Figure 2a displays the dependence of Γ_f to variations of the total horizontal wavenumber $K = \sqrt{k^2 + l^2}$ for three different values of the effective stratospheric shear $\tilde{\Lambda}_s$. In all cases Γ_f is found to be monotonically decreasing for increasing K. The coupling between the PVBs is therefore strongest for the longest waves and we can expect that a short-wave cut-off will appear at some value of K. Furthermore, Γ_f is identically zero if $\tilde{\Lambda}_s = \tilde{\Lambda}_t$, in which case $\bar{q}_y^d = 0$ [see (13)]. For even larger values of the stratospheric shear, Γ_f becomes negative and instability cannot occur.

The second requirement for instability is that the propagation speeds of the surface and tropopause PVBs should be 'sufficiently' equal. Figure 2b shows $(c_T - c_B)^2$ of (9) for the same cases as Fig. 2a. All three lines show a minimum at some finite value of K, marking the previously introduced 'resonant' wavenumber K_{res} (Ripa, 2001). For $K > K_{\text{res}}$, the surface/tropopause PVB tends to propagate more and more along with the basic-state velocity at the surface/tropopause. On the other hand, if $K < K_{\text{res}}$, the phase-speeds are more and more dominated by the presence of the surface/tropopause basic-state PV gradient. If these gradients have opposite sign, the phase-speed difference increases with decreasing K.

Comparing Figs. 2a and b one is able to specify the quoted word 'sufficient': The ratio of $(c_T - c_B)^2$ and Γ_f, shown in Fig. 2c, determines whether instability will set in. Only if this ratio is between zero and one, the NMs will form a growing/decaying pair. What is meant here physically is that if the phase-speed difference is small, Γ_f can be small as well (as long as it is of the correct sign). On the other hand, if the phase-speed difference is large, a strong coupling is necessary to destabilise the flow. Clearly, the short-wave cut-off results from a weakness of the coupling at large K. Less well known in the literature on the Eady model, but obvious from Fig. 2c is that at a sufficiently small wavenumber a long-wave cut-off is likely to appear. This will happen if the phase-speed difference increases more rapidly (with decreasing k) than the coupling-function. Only if $\tilde{\Lambda}_s = 0$ (dashed lines) there is no long-wave cut-off (similar to the classic Eady model with upper rigid lid). In all other cases both a short-wave and a long-wave cut-off exist.

5. Discrete normal modes

The principle effect of the added stratospheric layer is to modify the mean PV gradient at the tropopause [see (12)]. In this section, we explore the different situations which are possible. We use the values $\Lambda_t = 1$, $N_t^2 = 1$ and $N_s^2 = 4$ and vary the stratospheric 'effective' shear $\tilde{\Lambda}_s$ (and thereby $\bar{q}_y^d$). Insight in the PV vertical structure is obtained by showing in the figures, among others, the function $\mathcal{F}_3$ defined as ($\mathcal{F}_{1,2}$ follow later):

$$\mathcal{F}_3 = \frac{2\hat{T}}{\hat{T} + \hat{B}} = \frac{2\hat{T}/\hat{B}}{1 + \hat{T}/\hat{B}}, \tag{14}$$

where $\hat{T} = |T|$ and $\hat{B} = |B|$ are the absolute values of the amplitudes of the PVBs. The function $\mathcal{F}_3$ satisfies three easy-to-remember identities: $\mathcal{F}_3 = 0 \Leftrightarrow \hat{T}/\hat{B} = 0$, $\mathcal{F}_3 = 1 \Leftrightarrow \hat{T}/\hat{B} = 1$ and $\mathcal{F}_3 = 2 \Leftrightarrow \hat{T}/\hat{B} = \infty$.

5.1. Zero tropopause PV gradient: Marginal stability

The tropopause PV gradient $\bar{q}_y^d$ is zero if the 'effective' shears are equal, i.e. if $\tilde{\Lambda}_s = \tilde{\Lambda}_t$ [see (12)]. The flow is marginally stable to NM perturbations. This situation, which is displayed in Fig. 3a, will be our 'reference' case, since it resembles the semi-infinite extension of the Eady model where the upper boundary condition is applied at infinite height. Because $\bar{q}_y^d$ is zero, the coupling function Γ_f is also zero, and the NMs propagate as two uncoupled PVBs. In fact, the NM propagating with $c = c_B$ is a pure surface PVB with $\hat{T}/\hat{B} = 0$ (Fig. 3b). Its phase-speed

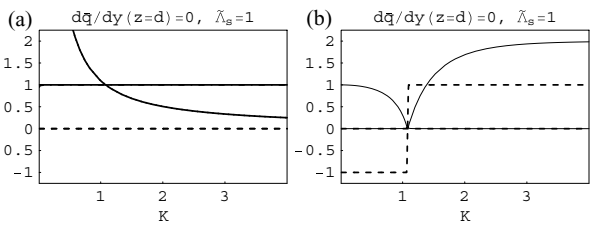

Fig. 3. (a) Real (full) and imaginary (dashed) part of the NM phase-speed for the reference case with $\bar{q}_y^d = 0$, as a function of the total horizontal wavenumber $K = \sqrt{k^2 + l^2}$. Tropospheric shear $\tilde{\Lambda}_t = 1$ and $N_s^2 = 4$. In the reference case, the two branches of the phase-speed meet at the resonant wavenumber $K = K_{\text{res}}$. (b) Displays amplitude and phase relations, $\mathcal{F}_3$ (full) and $\cos(\epsilon_T - \epsilon_B)$ (dashed).

c_B increases without bound as K is decreased to zero. Taking the $N_s^2 \to N_t^2$ or the $d \to \infty$ limit results in $c_B = \bar{u}_0 + \Lambda_t/\mu_t$, the classic result from the Eady model without the upper rigid lid (Gill, 1982).

The second NM in Fig. 3a propagates with the same speed as the tropopause PVB, $c = c_T = \bar{u}(z = d)$. This NM is identical to a continuum mode (CM) of the semi-infinite Eady model (De Vries and Opsteegh, 2005). To retain a time-independent structure, the CM is formed by a particular combination of the two PVBs. It depends on the wavenumber whether or not the CM is structurally similar to the tropopause PVB. For large K, the structures are similar (see full thin lines, $\mathcal{F}_3 \to 2$ as K increases). As K is decreased, the fraction $\hat{T}/\hat{B}$ also decreases. We can understand this quite easily. As long as $\hat{T} \neq 0$, the phase-speed must equal $\bar{u}_d$ under the constraint of an NM. The surface winds attributable to the tropopause PVB generate a surface edge wave, which in absence of the tropopause PVB would propagate with a different speed. For $K > K_{\text{res}}$ this speed is lower than that of the tropopause PVB. Therefore, the CM can only stand as an NM if the tropopause PVB helps the surface PVB to propagate zonally. This explains why there is zero phase-difference between surface and tropopause anomaly for $K > K_{\text{res}}$ (dashed line in Fig. 3b). Figure 4 schematically illustrates [in the spirit of Hoskins et al. (1985)] the effect of the tropopause PVB on the propagation speed of the surface PVB.

As K is decreased further, the surface PVB should be speeded up less and less ($\hat{T}/\hat{B}$ decreases further), until at $K = K_{\text{res}}$ the natural phase-speed of the surface PVB is equal to that of the tropopause PVB. A clear case of a resonant situation which cannot be structurally stable unless $\hat{T}/\hat{B} = 0$ ($\mathcal{F}_3 = 0$). Although the flow is marginally stable to exponentially growing NM perturbations, it is obvious that adding a tropopause PVB with $K \sim K_{\text{res}}$ would cause the surface edge wave to amplify in time (and to render the structure to be non-barotropic). The growth would be linear in time because there is no mutual interaction between the tropopause and the surface PVB.

For $K < K_{\text{res}}$, the surface PVB propagates faster in the eastward direction than the tropopause PVB does and therefore has to be slowed down to get a CM. The only way to achieve this is

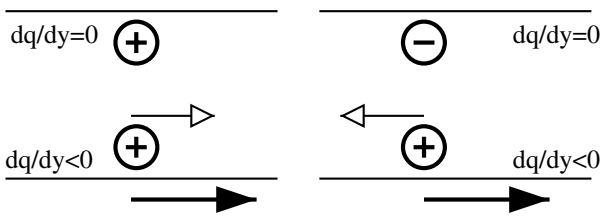

Fig. 4. The effect of the tropopause PVB on the propagation speed of the surface PVB. The long filled arrow indicates the natural phase-propagation of the surface PVB relative to the mean flow. The small arrow represents the effect of the tropopause PVB on the propagation speed of the surface PVB.

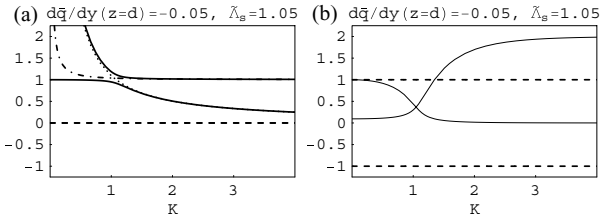

Fig. 5. As in Fig. 3a–b, but for a small negative value of $\bar{q}_y^d = -0.05$. Additionally to Fig. 3, panel (a) displays also the phase speeds of the PVBs, c_B (dotted) and c_T (dash-dot).

by giving the tropopause PVB the opposite phase of the surface PVB[3] (Fig. 4) and then to increase the fraction $\hat{T}/\hat{B}$. A limit situation is reached when K becomes zero. The uncoupled surface PVB would propagate eastward with infinite speed. The CM can only be formed if the total meridional wind at the surface is nearly zero. Using (A3) in the Appendix, this leads to $\hat{T} = \hat{B}$ ($\mathcal{F}_3 = 1$). Just enough meridional wind has been left over to guarantee a propagation speed of $c_T = U_d$.

5.2. *Negative tropopause PV gradient: NM stability*

If $\tilde{\Lambda}_s > \tilde{\Lambda}_t$, the tropopause PV gradient has the same sign as the surface PV gradient (Fig. 5). The flow is stable to NM perturbations of all wavelengths. The phase-speeds differ only slightly from the reference case. However, it is interesting to see that the NMs exchange 'identity' near the resonant wavenumber: The NM resembling the surface PVB becomes a CM and the NM resembling the tropopause PVB becomes a surface edge wave.

Again, this behaviour is understood most easily using the idea of helping and hindering the propagation (see Fig. 6a). On the short-wave side, the NM with $\hat{T}/\hat{B} \to 0$ ($\mathcal{F}_3 \to 0$) as $K \to \infty$ resembles the surface PVB. To stand as a mode, the phase-difference must be π for this NM (the eastward propagation speed of the tropopause PVB has to be reduced). When K decreases, the fraction $\hat{T}/\hat{B}$ must increase because the natural phase speed difference becomes smaller. At $K = K_{\text{res}}$, the natural phase-speeds of the PVBs (the dash-dot and dotted lines in Fig. 5a) are equal. For even smaller K the surface PVB propagates eastward more rapidly than the tropopause PVB. To stand as a mode, the fraction $\hat{T}/\hat{B}$ has to increase if the phase-difference is to be kept at π. When K decreases to zero, this NM more and more resembles the CM.

The second NM is formed by consequently retaining zero phase-difference, all the way down to $K = 0$. Using a similar reasoning its identity changes from a CM or tropopause PVB at high K to a surface edge wave at small K.

[3] Similar behaviour of the CM is noted in De Vries and Opsteegh (2005) in which the height of the CM is varied. In that case the surface PT anomaly changes sign if the CM is moved across the steering level.

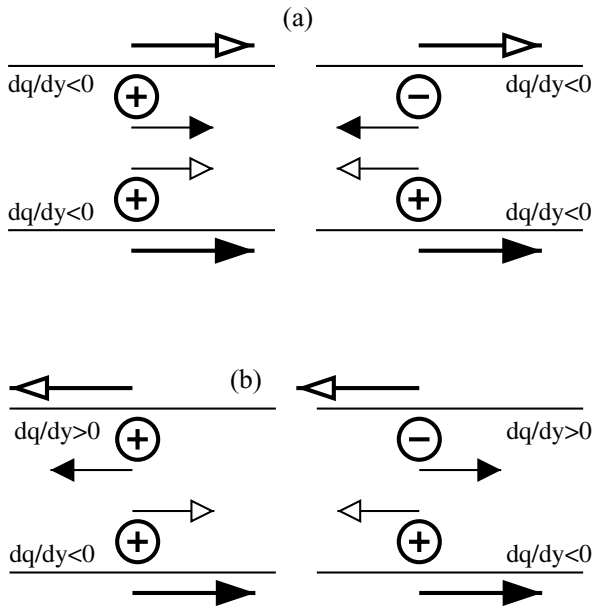

Fig. 6. Similar to Fig. 4 but a tropopause mean PV gradient of equal (a) and opposite (b) sign as the surface mean PV gradient. Long arrows indicate the natural phase-propagation of the PVBs relative to the mean flow, small arrows indicate the effect of the PVB at the opposite boundary (filled arrows represent the effect of the surface PVB, open arrows represent the effect of the tropopause PVB).

5.3. *Small positive tropopause PV gradient*

If $\tilde{\Lambda}_s$ is smaller than the tropospheric 'effective' shear $\tilde{\Lambda}_t$ (but still positive), the tropopause PV gradient becomes larger than zero [see (12)]. The Charney-Stern condition then predicts that growing NMs exist for a certain range of wavenumbers. The flow becomes unstable first for perturbations with a wavenumber equal to the resonant wave $K = K_{\text{res}} \sim 1$ (Fig. 7a). An explanation in terms of the arguments presented in Section 4.2 goes along the following lines. If the difference between the 'effective' shears is small, the PV gradient at the tropopause is small. As a result, the coupling-function Γ_f is small and the basic state will be unstable only if the propagation speeds of the PVBs match sufficiently (Fig. 7a), which is near the resonant wavenumber.

Both ultra-long and short-wave neutral NMs propagate like the CM and the surface edge wave of the reference case discussed in Section 5.1 above. However, the phase-difference of the NM resembling the surface edge wave is no longer arbitrary as in the reference case. For wavenumbers above the short-wave cut-off, both NMs have zero phase-difference [thin dashed line, $\cos(\epsilon_T - \epsilon_B) = 1$]. As the wavenumber is decreased and we enter the wedge of instability, the phase-difference increases and a pair of growing and decaying NMs is formed.[4] At the resonant point,

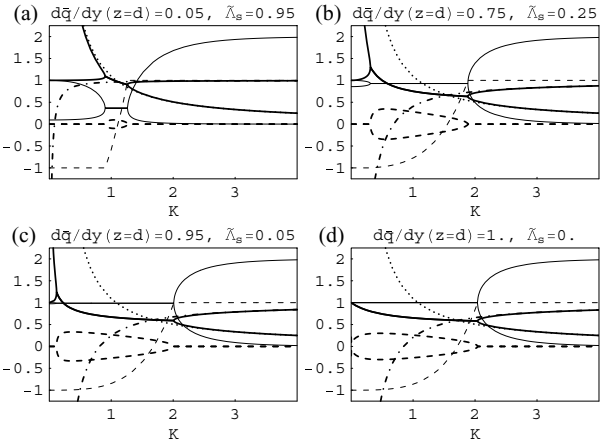

Fig. 7. Similar to Fig. 3, but for small positive values of $\bar{q}_y^d$. Real (full thick) and imaginary (dashed thick) part of the NM phase-speed as a function of K. Also shown are the phase-speeds of the PVBs, c_B (dotted) and c_T (dash-dot) as well as $\mathcal{F}_3$ (thin full lines) and cos $(\epsilon_T - \epsilon_B)$ (thin dashed line).

where $c_T = c_B$ (meeting point of the dotted and dash–dotted lines in Figs. 7a–d) it can be confirmed that the phase-difference (of both the GNM and the DNM) is indeed $\pi/2$. The phase-difference continues to increase until finally a phase-difference of π is reached at the long-wave cut-off. Within the wedge of instability, the amplitude ratio $\hat{T}^2/\hat{B}^2 = -\bar{q}_y^d/\bar{q}_y^0$ necessarily remains constant and – for this particular choice of the basic state – smaller than one. For K below the long-wave cut-off, the system can no longer satisfy both the condition that $\hat{T}^2/\hat{B}^2 = -\bar{q}_y^d/\bar{q}_y^0$ (required for uniform exponential amplification), and the condition of structural stability. Two neutral NMs are formed (both with phase-difference π). The first NM is the analogue of the surface edge wave ($\hat{T}/\hat{B}$ decreases as $K \to 0$ and the eastward phase-speed increases without bound). The second NM is the analogue of the CM. This NM has a finite eastward propagation speed of approximately $\bar{u}_d$ and a structure which approaches $\hat{T}/\hat{B} \to 1$ ($\mathcal{F}_3 \to 1$) as $K \to 0$. The NM can only propagate with a finite speed if the meridional winds at the surface and the tropopause are almost zero (the opposing open and filled arrows in Fig. 6b should nearly cancel).

Please note that the propagation speeds of the neutral NMs can also be predicted directly from (9). The neutral NMs propagate with a speed $c = \frac{1}{2}(c_B + c_T) \pm c_x$ where c_x is strictly positive for neutral NMs. The contribution to c from the average phase-speed of the surface and tropopause PVB, $\frac{1}{2}(c_B + c_T)$, will be infinitely positive (eastward) or negative (westward) as $K \to 0$, depending on the sign of the stratospheric shear (and thereby on the ratio of the mean PV gradients at the surface and tropopause). As $K \to 0$, the factor c_x also tends to infinity, and therefore at least one of the

[4]Note that if a growing-decaying pair of NMs has formed, the phase structure is such that $0 \le \epsilon_B \le \epsilon_T \le \pi$ for the GNM (the tropopause PVB lies westward of the surface PVB), and $0 \le \epsilon_T \le \epsilon_B \le \pi$ for the DNM.

NMs will have an infinite positive or negative propagation speed as $K \to 0$. It turns out (and it could be verified by systematic expansion) that the other NM retains a finite propagation speed as $K \to 0$.

When $\tilde{\Lambda}_s$ is decreased further (Figs. 7b–c), the domain of instability increases both at the short and at the long-wave side (Fig. 7b). Ultra-long NMs are neutral because the difference between the natural phase speeds of the PVBs is too large [cf. 9]. The 'see'-effect (the Rossby height increases as $K \to 0$) cannot prohibit this. Although the phase-speeds of the two neutral long-wave NMs are qualitatively similar to those of the surface edge wave and the CM of Section 5.1, their structure – in terms of the ratio $\hat{T}/\hat{B}$ – starts to become more and more identical as $\tilde{\Lambda}_s$ approaches zero. Although the structures are nearly identical – remember that both neutral NMs also have the same phase-difference – their propagation speeds are completely different. We postpone an explanation of this apparently inconsistent result to Section 5.5.

A limit case is reached for $\tilde{\Lambda}_s = 0$ (Fig. 7d). The PV gradient at the tropopause is of equal amplitude as and of opposite sign to the surface PV gradient and the GNM has an amplitude ratio $\hat{T}^2/\hat{B}^2 = -\bar{q}_y^d/\bar{q}_y^0 \equiv 1$. This case, which has been investigated before by Rivest et al. (1992), can therefore be considered as the generalisation of the Eady model with upper rigid lid. The flow is unstable to perturbations of all wavenumbers smaller than the cut-off. The increase of the coupling-function Γ_f as $K \to 0$ (the 'see'-effect) counteracts the formidable increase of the phase-speed difference as $K \to 0$. A noticeable difference with the classic Eady problem with upper rigid lid is that the propagation speed $c_r = \frac{1}{2}(c_B + c_T)$ of the growing and decaying NMs becomes dispersive and approaches $c_r = \bar{u}(d)$ as $K \to 0$. For the classic problem, c_r is given by $c_r = \frac{1}{2}[\bar{u}(0) + \bar{u}(d)]$ for all growing and decaying NMs. In the present two-layer case, c_r always exceeds the value $\bar{u}_d/2$.

5.4. Large positive tropopause PV gradient

If the stratospheric shear becomes negative, (12) implies that $\bar{q}_y^d > -\bar{q}_y^0$ (remember that the gradients are of opposite sign). On the short-wave side, the interpretations are as before (Figs. 8a–d) and both a surface edge wave and a CM exist and they are nearly identical to the pure surface and tropopause PVB. At the long-wave side of the wedge of instability, again two neutral NMs form with both a phase-difference of π. As before, only one of the long-wave neutral NMs attains a finite eastward propagation speed as $K \to 0$. The other neutral NM propagates rapidly westward as K is decreased. Its amplitude ratio $\hat{T}/\hat{B}$ exceeds unity ($\mathcal{F}_3 > 1$) for all wavenumbers below the long-wave cut-off.

Let us turn to the NM which has a finite propagation speed. To 'speed up' the tropopause PVB in the eastward direction, the phase-difference is set to π and the ratio $\hat{T}/\hat{B}$ is decreased. Easily seen from Fig. 6b is that the surface PVB is simultaneously

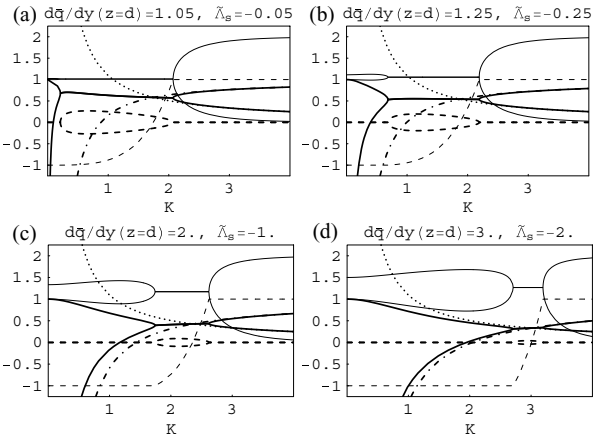

Fig. 8. Similar to Fig. 3, but for large positive values of $\bar{q}_y^d$. Drawing conventions as in Fig. 7.

slowed down in its eastward propagation. The combination retains a finite propagation speed and approaches the CM limit ($\hat{T}/\hat{B} \to 1$) as K decreases. For small negative stratospheric shear, the difference with the westward propagating NM is almost indiscernible (in terms of $\hat{T}/\hat{B}$) although the differences are huge in terms of phase-speed. The situation is similar to the previous section for $\tilde{\Lambda}_s$ slightly larger than zero. An explanation follows in the next section.

If the stratospheric shear attains larger negative values, the width of the domain of instability decreases and moves toward higher wavenumbers. Eventually, the cut-off propagates beyond the standard short-wave cut-off of the rigid lid Eady model (Figs. 8c–d). This occurs because the propagation speeds of the pure PVBs are almost equal for these short waves and the NM can grow even though the coupling-function is relatively weak at large K. As $\tilde{\Lambda}_s \ll 0$, the growth rate of the growing NMs decreases to zero, although the Charney-Stern condition for instability remains satisfied for all values $\tilde{\Lambda}_s < \tilde{\Lambda}_t$. Finally, note that the eastward propagation speed $c_r = \frac{1}{2}(c_B + c_T)$ of the growing and decaying NM is reduced as $\tilde{\Lambda}_s$ becomes more negative.

5.5. On the phase-speed of the long neutral NMs

In the previous sections we have seen that the neutral branches of the NMs, which form for different choices of the tropopause mean PV gradient, can be understood as modifications of Section 5.1. At the short-wave side, the NMs are similar to the surface edge wave and the tropopause CM, both in structure and in propagation speed. At the long-wave side of the domain, one of the two NMs approaches the CM limit of $c = \bar{u}(d) = 1$ and $\hat{T}/\hat{B} = 1$ ($\mathcal{F}_3 \to 1$), irrespective of the sign of the stratospheric shear. This leads to the idea that phase-speed of this NM is not determined primarily by the stratospheric shear, but by the structural differences between the PVBs instead. Figure 9 shows the difference $\phi_B(z) - \phi_T(z)$ of the PVB stream-functions (with

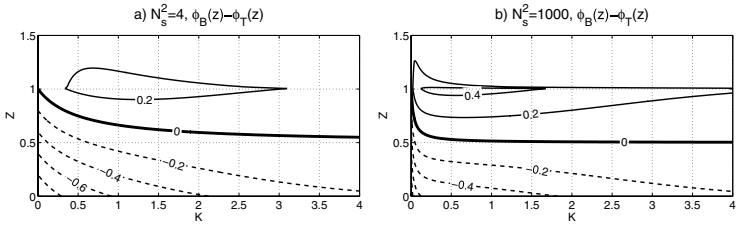

Fig. 9. The difference $\phi_B(z) - \phi_T(z)$ between the stream-functions of PVBs (with equal amplitude $\hat{B} = \hat{T} = 1$) as a function of K and z for two different stratifications.

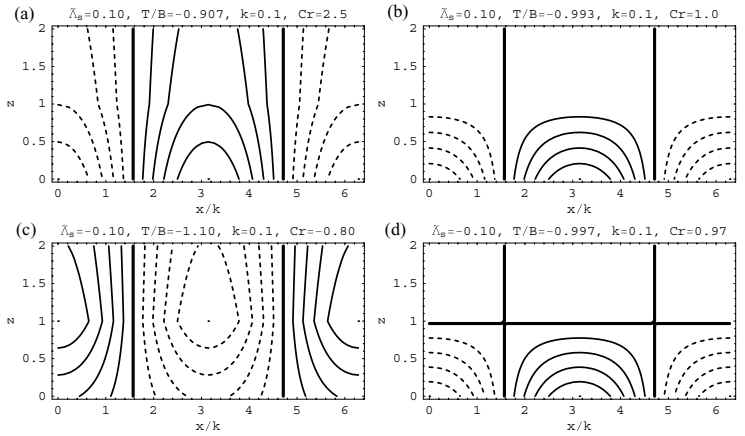

Fig. 10. Typical structure of the long-wave neutral NMs ($k = 0.1$, $\tilde{\Lambda}_t = 1$ and $N_s^2 = 4$). (a–b) Small positive stratospheric shear. (c–d) Small negative stratospheric shear. The thick line represents the zero contour, negative values have been dashed. Contourinterval: 0.2.

$\hat{B} = \hat{T} = 1$) as a function of the total horizontal wavenumber and the height for two different stratifications. The most important feature in Fig. 9a is the zero contour (thick line), which approaches $z = d$ as K decreases toward zero. From this we may infer that, if an NM forms with $\hat{T}/\hat{B} = 1$, this NM will propagate with a speed $\bar{u}(d)$ in the limit $K \to 0$, independent of the sign of the shear in the stratosphere. This property is lost in the rigid lid approximation (see Fig. 9b for the situation of a near-rigid lid).

The second long-wave neutral NM has a $K \to 0$ asymptotic propagation speed that is entirely different. Its propagation speed becomes infinitely positive (eastward) or negative (westward) as $K \to 0$, depending on whether the stratospheric shear is positive or negative, respectively. Although the propagation speed of this NM differs greatly from that of the NM resembling the CM, its structure in terms of $\hat{T}/\hat{B}$ is not necessarily very far from unity (in which case the propagation speed would remain finite as $K \to 0$).

This apparent inconsistency is understood as follows. As K is decreased, the stream-function structures of the PVBs become less evanescent with height. A PVB of a given amount of total kinetic energy will therefore be associated with a PV anomaly of a smaller and smaller amplitude as K decreases. In the limit of $K \to 0$, the structures will have negligible PV whereas the stream-function remains finite. Such small PV anomalies (in terms of amplitude) can be advected very fast on a mean PV gradient of finite amplitude. A fraction $\hat{T}/\hat{B}$ deviating only slightly from unity, will therefore be enough to give the NM a very high propagation speed. If $\hat{T}/\hat{B} > 1$ the NM is dominated by the tropopause PVB, and propagates westward if the mean PV gradient at the tropopause exceeds the (absolute) value of the mean PV gradient at the surface (which occurs only if $\tilde{\Lambda}_s < 0$). If $\hat{T}/\hat{B} < 1$ (which occurs for basic states satisfying $\tilde{\Lambda}_s > 0$) the opposite happens and an eastward propagating NM is obtained. The above considerations can be verified graphically from Fig. 10.

6. Continuum modes

The PVB view can also be used to investigate the continuum modes (CMs) of the two-layer Eady model. Continuum modes are neutral, purely propagating modal structures characterised by non-zero PV at one interior level $z = h$. Because the interior PV can be located anywhere in the interior, a continuum of such CMs exists for in-viscid flows. CMs are required to properly describe the evolution of the general initial-value experiment (Pedlosky, 1964). Partly because of their neutrality, the CMs have been neglected mostly in the analytic literature, but interest in the CM has been increasing since the work of Farrell (1982) on non-modal and optimal growth (see e.g. Farrell, 1984; Morgan and Chen, 2002; De Vries and Opsteegh, 2005). This renewed attention is motivated by the fact that the CM causes a resonance if its propagation speed matches with the speed of one of the neutral discrete NMs (Thorncroft and Hoskins, 1990; Chang, 1992).

As said above the CM is characterised by non-zero PV at one interior level $z = h$. This interior PV anomaly takes the special form of a Dirac delta function

$$q(z = h) = Q\delta(z - h)e^{ikx}, \tag{15}$$

where $Q = \hat{Q} = 1$ will be taken from here. In the spirit of the previous sections, we will call the interior PV anomaly an interior PVB. If the mean PV gradient is zero in the interior, the CM must be a neutral wave that propagates with the speed of the basic flow at the level of the interior PV. To propagate with this speed, the CM is formed by the interior PVB and a surface and tropopause PVB in a specific ratio. The required baroclinic neutrality of the CM constrains the phase differences of the three PVBs to be fixed at zero or $\pm\pi$, resulting in a purely barotropic stream-function.

Since any combination of surface and tropopause PV can be represented by a linear superposition of the two discrete NMs, the CM can be viewed alternatively as an interior PVB in superposition with two discrete NMs. This alternative view facilitates the interpretation of the structure of the CM to be discussed below.

6.1. Resonant solution

The system of equations is singular for PV perturbations at the steering level of the neutral discrete NMs. In this case a resonant configuration is reached and part of the stream-function of the so-called resonant CM amplifies linearly in time. This linear resonance has been reported for the Eady model, see for instance Thorncroft and Hoskins (1990); Chang (1992); Davies and Bishop (1994); De Vries and Opsteegh (2005). The analytical properties of the classic rigid lid Eady model are discussed in more detail by Jenkner and Ehrendorfer (2006). The two-layer Eady model considered in the present paper is especially interesting (and different from the classic model of Jenkner and Ehrendorfer (2006)) because of the occurrence of multiple steering levels if the stratospheric shear of the basic state is negative. The 'asymmetric' surface and tropopause PV gradients alter the long-wave structure of the continuum modes in an essential way and long-wave resonating solutions may be found in the two-layer model, whereas they are absent in the classic model with rigid lid (Jenkner and Ehrendorfer, 2006).

6.2. PV structure

Figures 11 and 12 show the PV structure of the CMs for two particular cases with positive and negative stratospheric shear respectively. The structure is visualised by contour maps of $\mathcal{F}_1 := 2B/(\hat{B} + \hat{Q})$ as a function of K and the position of the interior PVB. The function $\mathcal{F}_1$ maps all possible ratios B/Q in the range $[-2, 2]$, and satisfies the simple relations $\mathcal{F}_1 = 0 \Leftrightarrow B/\hat{Q} = 0$, $\mathcal{F}_1 = \pm 1 \Leftrightarrow B/\hat{Q} = \pm 1$ and $\mathcal{F}_1 = \pm 2 \Leftrightarrow B/\hat{Q} = \pm\infty$. In a similar way also $\mathcal{F}_2 := 2T/(\hat{T} + \hat{Q})$ is plotted. From $\mathcal{F}_1$ and $\mathcal{F}_2$ we can infer the sign between T and B. Finally also $\mathcal{F}_3 = 2\hat{T}/(\hat{T} + \hat{B})$ (see 14) is shown. The steering levels of the discrete NMs are indicated by thick black

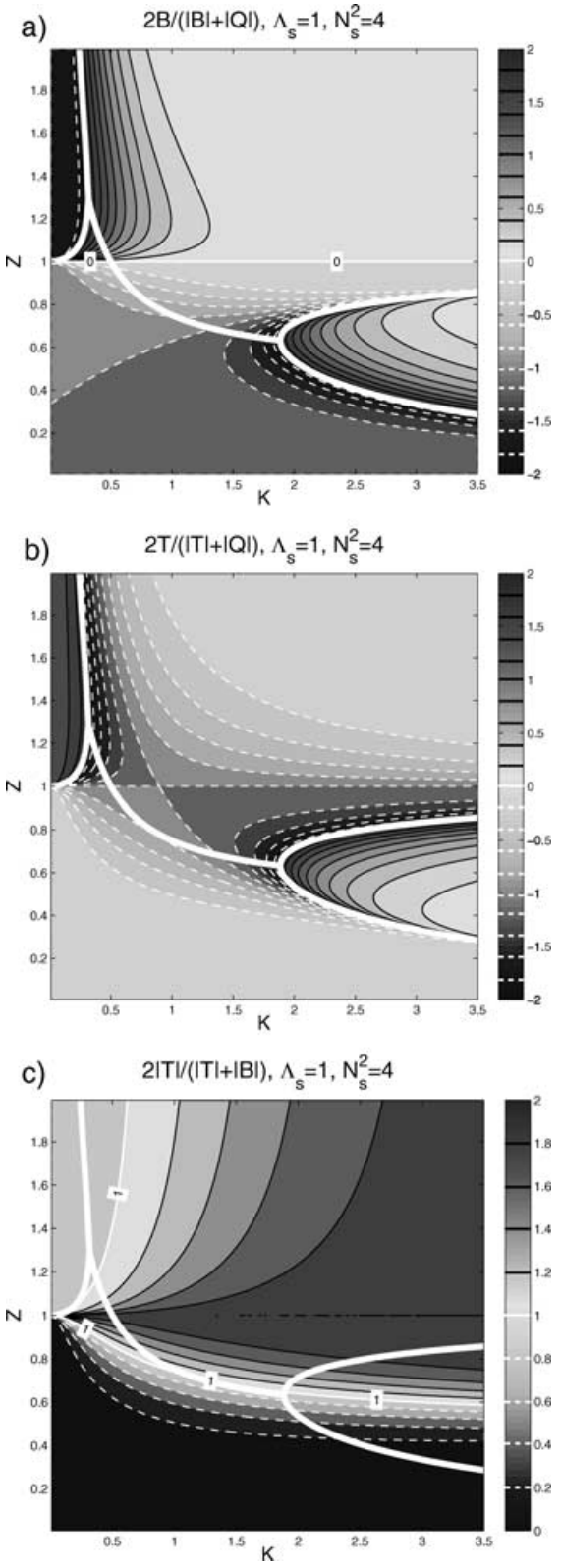

Fig. 11. Structure of the CMs for positive stratospheric shear $\Lambda_s = 1$. Thick full white lines mark the steering levels. Contour interval 0.20, negative contours are white and have been dashed for clarity.

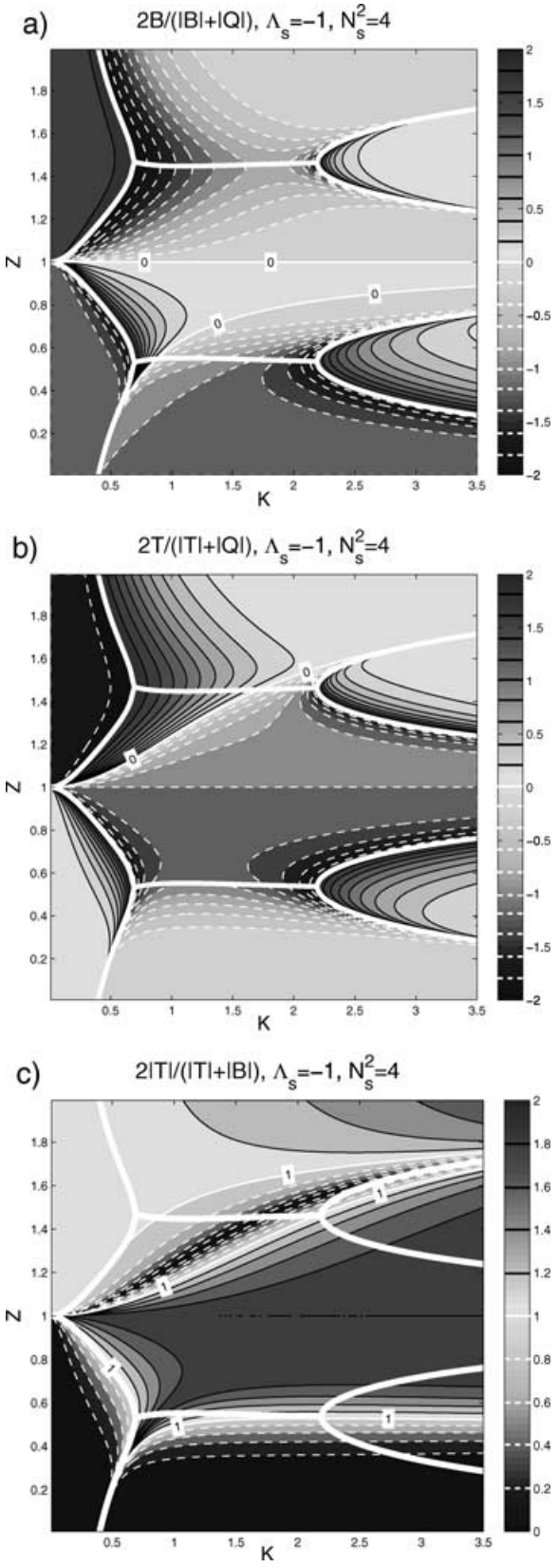

Fig. 12. As in Fig. 11 but for negative stratospheric shear $\Lambda_s = -1$.

lines. In the case of negative stratospheric shear (Fig. 12) more than two steering levels can occur for a given value of the wavenumber.

The amplitude ratios vary smoothly under variations of K and z, except if the interior PVB is moved across one of the steering levels of the neutral branches of the discrete NMs. In such a crossing, whether it is induced by wavenumber modification or by repositioning of the interior PVB in the vertical, both the surface and tropopause PVB change sign. The singular behaviour of the CMs near the neutral branch of the steering levels ($\mathcal{F}_1, \mathcal{F}_2 \to \pm 2$, i.e. both B/Q and T/Q become infinitely large, or $Q \to 0$ for finite B and T) is a direct consequence of the requirements that the CM remains neutral and propagates at a particular speed. However, although $\hat{T}/\hat{Q}$ and $\hat{B}/\hat{Q}$ become very large near the neutral steering levels, $\hat{T}/\hat{B}$ remains finite and approaches the value of the nearby discrete NM (see Figs. 11c and 12c), showing that the resonance is associated with only one of the two NMs. In contrast, the blow up of the ratios and the sign changes do not occur if the CM crosses a critical level, i.e. the unstable part of the steering level. Can we understand these transition-differences?

6.3. Crossing a steering level

6.3.1. Short waves. The two discrete neutral NMs are barotropic and non-amplifying solutions to the dynamical equations, each propagating with a specific propagation speed. So, if we want to create a modal structure that is neutral and has a barotropic stream-function and that moreover propagates with a speed equal to one of the neutral steering levels, we choose either one of the two discrete NMs (and choose $\hat{Q} = 0$ of the interior PVB). It is clear that any non-zero interior PVB placed at one of the steering levels will cause a resonance similar to the resonance in the rigid lid Eady model (Chang, 1992; Jenkner and Ehrendorfer, 2006).

Modification of the phase-speed can be achieved by introducing a small-amplitude interior PVB at the level where the basic zonal flow matches the desired propagation speed. In this way the discrete NM is 'converted' into a CM. In general, the interior PVB will excite both neutral discrete NMs via its wind-field and as a result the CM will be composed (in addition to the interior PVB) of both discrete NMs. However, the structure of short-wave CMs nearby a steering level can be figured out by considering the CM as being a modified discrete NM.

Let us illustrate this with an example. We start with the most slowly eastwardly propagating discrete NM at wavenumber $k = 3.0$. This NM is characterised by B and T of equal sign (see Figs. 7b and 8b for the structure of this mode). Because $\hat{B}/\hat{T} \gg 1$ for this NM we may neglect the tropopause PVB to first approximation. If we locate the interior PVB above the steering level (Figs. 11 and 12) the discrete NM must be slightly accelerated in the eastward direction. To achieve this, the interior PVB

therefore should have (1) a small amplitude (leading to large $\hat{B}/\hat{Q}$ and $\hat{T}/\hat{Q}$) and (2) the same sign[5] as B. Both features are indeed observed in Figs. 11 and 12. What happens at the tropopause in this example? If the positive maximum of the interior PVB is positioned below the tropopause PV maximum, the interior PVB accelerates the small-amplitude tropopause PVB (associated with the discrete NM satisfying $\hat{B}/\hat{T} \gg 1$) in the westward direction. This situation inevitably leads to a non-barotropic stream-function and thus must be compensated for. This is achieved by slightly increasing the amplitude of the tropopause PVB (and – in effect – thus exciting the second discrete NM, which has $\hat{T}/\hat{B} \gg 1$ and thus hardly influences the surface PVB).

What we learn from the example above, is that although both discrete NMs and an interior PVB are involved in the short-wave CM, its structure can be anticipated qualitatively from a consideration of the dominant contributions of the nearby neutral discrete NM. The other short-wave CMs and steering-level crossings can be understood analogously.

6.3.2. Long waves. At the long-wave side of the domain, however, the above heuristic derivation of the CM structure does not hold any longer. This can be seen already from the fact that both discrete NMs have $\hat{T}/\hat{B}$ ratios not far from unity, indicating that the PVBs are strongly coupled (because of the huge Rossby height at small K). The main observation that both B and T change sign as the interior PVB is moved across the steering level, however, does hold at small K. We note a number of interesting properties of the long-wave neutral CMs:

(1) Long-wave tropospheric CMs for $\Lambda_s = 1$ have almost zero tropopause PV (Figs. 11b–c) but an interior PVB of comparable amplitude but of opposite sign as the surface PVB. This is understandable since a long-wave surface PVB in isolation would propagate eastward very rapidly.

(2) Long-wave stratospheric CMs for $\Lambda_s = 1$ have negligible interior PV but large, almost equal amplitude B and T of opposite sign. As a result the stream-function cancels in a large domain and the interior PVB can have a strong effect on the propagation despite its relatively small amplitude. This result should be contrasted to the short-wave stratospheric CMs far away from the steering levels of the discrete NMs. Those CMs are almost purely interior PVBs (Figs. 11a–b and 12a–b).

(3) In contrast to (1) above, the long-wave tropospheric CMs come in two different types in the case of negative stratospheric shear $\Lambda_s = -1$; those with large and small $\hat{T}/\hat{B}$ fractions (Fig. 12c, the $\hat{T} = \hat{B}$ contour roughly follows the upper steering level). As in point (1) above, if $\hat{T}/\hat{B} \ll 1$ the surface PVB is most important and Q is positioned such that it hinders the rapid eastward propagation of B (B and Q are π out of phase). On the other hand, if $\hat{T}/\hat{B} \gg 1$, Q must hinder the rapid westward propagation of T (Q and T are π out of phase).

[5]To decrease the eastward phase-speed (moving the interior PVB down in the figures), one should obviously introduce an interior PVB of opposite sign as B.

6.4. Crossing a critical level

The following question arises. What is the reason that the singular behaviour observed in the previous section does not occur if we cross a critical level? Appendix B shows the expressions underlying the ratios plotted in Figs. 11 and 12. From the mathematical point of view [cf. eqs (B1–B2)] it is entirely clear that singularities will not occur if the discrete NMs form a complex-conjugate pair. Moreover, from Fig 11c and 12c we see that the ratios $\hat{T}/\hat{B}$ vary continuously with the parameters in the complete domain. Can we understand the physical reason underlying these results?

If the discrete NMs form a growing/decaying pair, the modal ingredients to construct a neutral modal structure are the GNM and the DNM, which both have a baroclinic stream-function. It is easily verified that a barotropic structure is obtained only if the amplitudes in front of the discrete NMs form a complex-conjugate pair, just as the discrete NMs themselves.

However, to keep an initially barotropic structure -composed of the GNM and DNM – untilted as time progresses requires a non-zero interior PVB at the critical level. (From a modal perspective this is entirely clear since the DNM decays and the GNM grows which is a structurally unstable situation.) Notice that this interior PVB is needed even though the discrete NMs themselves propagate with the same speed (unlike in the neutral regimes). Both the singular behaviour and the resonances do not occur. This is entirely different from the case in which the discrete NMs are neutral. Whereas we find non-amplifying neutral discrete NMs but resonant CMs in the stable regime, the unstable regime provides us with exponentially growing and decaying NMs but no resonant CMs.

If the position of the interior PVB of the CM is changed smoothly, we see that the ratios B/Q and T/Q also change smoothly and may even transit through zero (Figs. 11a–b and 12a–b). If B (or T) vanishes for a given CM configuration, it is clear that the meridional wind-field must also be zero at the level of B (or T). For example, in Fig. 12a there is a tropospheric zero-line. CMs at this line have zero PT perturbation at the surface and zero meridional wind.

7. Summary and final remarks

In the previous sections we have examined the effects of replacing the upper rigid lid by a stratospheric layer with a different shear and a different buoyancy frequency. The differences between the two layers introduce a basic-state PV gradient at the tropopause, $\bar{q}_y^d$, which is in general not equal to the PV gradient at the surface, $\bar{q}_y^0$. Whether the NMs are neutral or growing for a certain wavenumber depends on the sign and the size of the PV

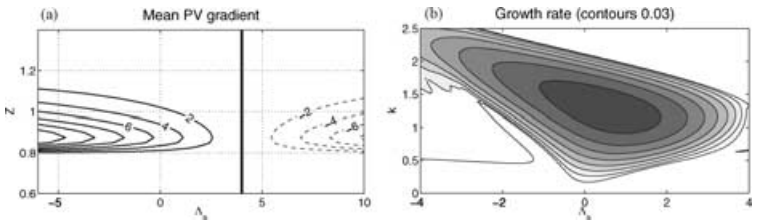

Fig. 13. Results for a smoothed basic state. (left) Meridional PV gradient (in contours) as a function of Λ_s for $N_t^2 = 1, N_s^2 = 4$ and $\Lambda_t = 1$. The thick line indicates the zero contour. (right) Growth rates kc_i of the GNM of the smoothed basic state (using a 2nd-order finite-difference scheme).

gradients at the surface and tropopause as well as on the Rossby-height. The results have been interpreted in terms of a coupling between a surface and tropopause PVB, a perspective which is analogous to the counter-propagating Rossby wave (CRW) view on baroclinic instability (Bretherton, 1966; Hoskins et al., 1985; Heifetz et al., 2004a). We summarise the main results.

(1) If the tropopause PV gradient $\bar{q}_y^d$ is zero, the basic state is marginally stable to NM perturbations and the model resembles the Eady model with the upper rigid lid removed. Two neutral NMs exist. One is a pure surface edge wave, the other is a continuum mode (CM) with a particular distribution of PV at the tropopause and PT at the surface. If the PV gradients at the surface and the tropopause have the same sign, the Charney-Stern (1962) theorem predicts that all NMs are neutral.

(2) If the tropopause PV gradient $\bar{q}_y^d$ is smaller than and of opposite sign as the surface PV gradient $\bar{q}_y^0$, the flow is unstable to NMs of wavenumbers between a short- and a long-wave cut-off. The short-wave cut-off is analogous to the classic Eady model with upper rigid lid and originates from a consideration of the Rossby height. The long-wave cut-off appears because the difference between the natural propagation speeds of the PVBs becomes too large (in this case because the ultra-long surface PVB propagates too rapidly in the eastward direction). Therefore, the tropopause PVB cannot form a configuration with the surface PVB which is both phase-locked and growing. Increasing the tropopause PV gradient $\bar{q}_y^d$ (keeping $0 < \bar{q}_y^d < -\bar{q}_y^0$), reduces the phase-speed of the long-wave surface PVB and growing NMs are found for a wider range of wavenumbers.

(3) A limit case is reached if the surface and the tropopause PV gradients have equal (but opposite sign) amplitude, $\bar{q}_y^d = -\bar{q}_y^0$. The flow is now unstable to all NMs longer than the short-wave cut-off. The short-wave cut-off depends on the exact value of N_s^2 that is considered. In the limit $N_s^2 \to \infty$ the classic Eady model with upper rigid lid is recovered.

(4) If the $\bar{q}_y^d$ becomes larger than $-\bar{q}_y^0$, the long-wave cut-off reappears. Ultra-long NMs are neutral. In this case the long-wave tropopause PVB propagates too rapidly to the west to be able to form an NM which is both phase-locked and growing. A pair of neutral NMs exists, one resembling the tropopause PVB, the other a continuum mode.

(5) The structure of the continuum modes (CMs) can also be explained using the PVB perspective. These modal structures characterised by non-zero PV at an interior level (as well as by non-zero PV at the surface and tropopause) are neutral even if the discrete NMs are unstable, but may cause resonances if they are located on the steering level of the neutral discrete NMs. In case the stratosphere has negative shear, steering levels occur also in the stratosphere, which then lead to multiple resonant levels.

We end this paper with some remarks. At first sight, the simplistic description of the troposphere stratosphere transition (the tropopause) can be questioned. In the present paper the tropopause is simulated by both a discontinuity of the basic-state buoyancy frequency N^2 and a discontinuity in the vertical shear Λ of the zonal wind $\bar{u}$. In reality the troposphere-stratosphere transition is smooth. To examine the effect of this smoothing, we have adjusted N^2 and $\bar{u}$ in a region $d - h < z < d + h$ (with $h = 0.2$ the half-width of the smoothing region) such that the N^2 and $\bar{u}$-profiles are smooth (continuous and differentiable) in the complete domain. The smoothing introduces a non-zero PV gradient in the complete smoothing domain.[6] This PV gradient has been plotted in Fig. 13. The over-all sign of the PV gradient within the smoothing region varies in the same way with Λ_s as the singular contribution $\bar{q}_y^d$ [see (12)] did. If $\tilde{\Lambda}_s = 1$, the PV gradient vanishes in the complete smoothing region implying that the model resembles the semi-infinite extension of the Eady model. If $\tilde{\Lambda}_s \geq 1$, the PV gradient at the tropopause has the same sign as the PV gradient at the surface, which implies that the smoothed basic state is neutral. On the other hand, if $\tilde{\Lambda}_s < 1$, the sign of the PV gradient is different at the surface and at the tropopause region and we expect the existence of a pair of growing and decaying NMs. Fig. 13b confirms that growth rates obtained for the smoothed basic state are similar to the results obtained before by Müller (1991).

Another point of concern relates to the physical relevance of the obtained long-wave modal structures. Since the present study is based on an f-plane approximation, very low wavenumbers can hardly be justified without making large errors. It is expected that NM results will also be modified if a β-plane approximation is made, and modes resembling CMs will necessarily have a more complex vertical PV structure. Nevertheless the present paper hopefully contributes to the qualitative understanding of baroclinic instability and the various wave structures supported by different types of basic states.

[6]The simple smoothing approximates $N^2(z)$ by a third-order polynomial and $\bar{u}(z)$ by a fourth order polynomial. This gives nine degrees of freedom to solve the nine constraints [$\mathrm{d}\bar{q}/\mathrm{d}y$ continuous (#2); N^2 smooth (#4); $\bar{u}$ smooth but unbounded at infinity (#3)].

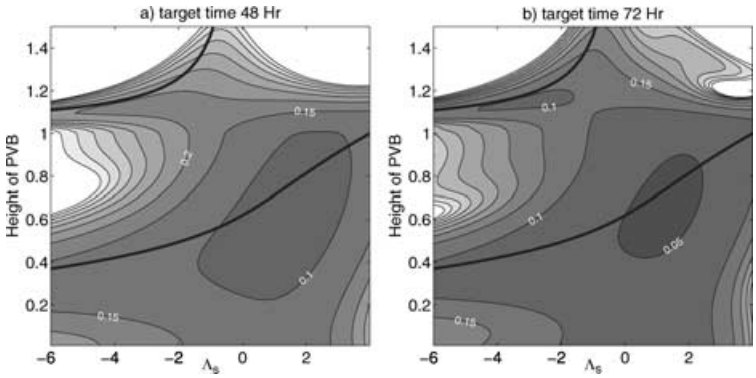

Fig. 14. Amount of PV needed initially at level h (vertical axis) to produce surface winds of 30 m s^{-1} after a certain target time. (a) target time 48 h; (b) target time 72 h. Thick black lines indicate steering levels. The basic state is specified by $N_s^2/N_t^2 = 4$, $\Lambda_t = 1$ and $d = 1$.

To conclude, in some respect linear NM instability theory provides only a starting point for the understanding of the development of atmospheric disturbances. As an example of the variations in non-modal development occurring in the two-layer Eady model, Fig. 14 displays the amount of PV that is initially needed at a single level [in the form of an interior PVB $q(t = 0) = Q\delta(z - h)\exp(ikx)$] to generate surface winds of 30 m s^{-1} at a given target time. For each value of Λ_s we have taken the wavenumber k that produces the most rapidly growing NM. This is merely a choice and will not necessarily produce optimal growth (Heifetz and Methven, 2005). The panels show clearly that the region near the tropospheric steering level is favoured for surface development. Although, as discussed in the previous section, there is no resonantly growing CM, the PVB at the steering level still favours the excitation of the GNM. At high altitudes, more PV is required. However, some regions in the stratosphere -associated with the stratospheric steering level- are also amenable to surface growth. Moreover, even in situations in which the NMs are practically neutral (for instance near $\Lambda_s = 4$), the non-modal development can be strong.

The above observations show that growth-mechanisms differing from conventional normal-mode baroclinic instability (such as resonant growth due to near-steering level interior PVBs) can play an important role in situations with rapid development, in line with existing studies (Farrell, 1984; Davies and Bishop, 1994; Heifetz et al., 2004a; Dirren and Davies, 2004; De Vries and Opsteegh, 2005; Heifetz and Methven, 2005; De Vries and Opsteegh, 2006). Further research is required to assess the importance of such intrinsically non-modal growth mechanisms for the more realistic flow configurations amenable to an interpretation in terms of counter-propagating Rossby waves (Methven et al., 2005a,b).

Appendix A: Properties of the PVBs

The surface and tropopause PVB provide a physically intuitive basis for the discrete NMs. They are analogous to the CRWs of Heifetz et al. (2004a) constructed using the home-base method. The PVBs have unit perturbation PV either at the surface (B) or at the tropopause (T), i.e. $q_B(z) = \delta(z)$ and $q_T(z) = \delta(z - d)$. We write $\phi(z) = B\phi_B(z) + T\phi_T(z)$ for the total stream-function of the NM, where B and T are complex amplitudes. The PVB stream-functions are given by

$$\phi_B(z) = \frac{H(d-z)}{\alpha}\left\{\tilde{\mu}_s \sinh[\mu_t(z-d)] - \tilde{\mu}_t \cosh[\mu_t(z-d)]\right\} - \frac{H(z-d)}{\alpha}\{\tilde{\mu}_t \exp[-\mu_s(z-d)]\}, \tag{A1}$$

$$\phi_T(z) = \frac{H(d-z)}{\alpha}\left[-\tilde{\mu}_t \cosh(\mu_t z)\right] - \frac{H(z-d)}{\alpha}\left\{\tilde{\mu}_t\gamma_2 \exp[-\mu_s(z-d)]\right\}, \tag{A2}$$

where $H(x)$ is the Heaviside step-function, $\mu_t = N_t K$, $\mu_s = N_s K$, $\tilde{\mu}_T = K/N_t$ and $\tilde{\mu}_s = K/N_s$, with $K = \sqrt{k^2 + l^2}$ the total horizontal wavenumber. Furthermore, $\alpha = \tilde{\mu}_t(\tilde{\mu}_t\gamma_1 + \tilde{\mu}_s\gamma_2)$ where $\gamma_1 = \sinh(\mu_t d)$ and $\gamma_2 = \cosh(\mu_t d)$. We note the following relations:

$$\frac{\phi_T(d)}{\phi_B(d)} = \gamma_2, \quad \frac{\phi_B(0)}{\phi_T(0)} = \gamma_2 + \frac{N_t}{N_s}\gamma_1, \quad \phi_T(0) = \phi_B(d). \tag{A3}$$

The phase-speeds of the PVBs and their couplings are given by:

$$c_B = \bar{u}_0 + \left(\frac{\partial\bar{\theta}}{\partial y}\frac{\phi_B}{\theta_B}\right)_{z=0}, \quad f_B = -\left(\frac{\partial\bar{\theta}}{\partial y}\frac{\phi_T}{\theta_B}\right)_{z=0}, \tag{A4}$$

$$c_T = \bar{u}_d + \left(\frac{\partial\bar{q}}{\partial y}\frac{\phi_T}{q_T}\right)_{z=d}, \quad f_T = -\left(\frac{\partial\bar{q}}{\partial y}\frac{\phi_B}{q_T}\right)_{z=d}. \tag{A5}$$

Explicit expressions are expressed most easily in terms of the 'effective' shears $\tilde{\Lambda}_t = \Lambda_t N_t^{-2}$ and $\tilde{\Lambda}_s = \Lambda_s N_s^{-2}$:

$$c_B = \bar{u}_0 + \frac{\tilde{\Lambda}_t}{\tilde{\mu}_t}\left(\frac{\tilde{\mu}_t\gamma_2 + \tilde{\mu}_s\gamma_1}{\tilde{\mu}_t\gamma_1 + \tilde{\mu}_s\gamma_2}\right), \tag{A6}$$

$$c_T = \bar{u}_d - \left(\frac{\tilde{\Lambda}_t - \tilde{\Lambda}_s}{\tilde{\mu}_t}\right)\left(\frac{\tilde{\mu}_t\gamma_2}{\tilde{\mu}_t\gamma_1 + \tilde{\mu}_s\gamma_2}\right), \tag{A7}$$

$$f_B = \frac{-\tilde{\Lambda}_t}{\tilde{\mu}_t\gamma_1 + \tilde{\mu}_s\gamma_2}, \quad f_T = \frac{\tilde{\Lambda}_t - \tilde{\Lambda}_s}{\tilde{\mu}_t\gamma_1 + \tilde{\mu}_s\gamma_2}, \tag{A8}$$

where $\bar{u}_0 = \bar{u}(z = 0)$ and $\bar{u}_d = \bar{u}(z = d)$.

Appendix B: Analytical structure of the CM

By writing $\psi(z) = \int G(z, z')q(z')\mathrm{d}z'$, a Green's function approach is adopted to derive expressions for the CM streamfunction. The function $G(z, z')$ has been defined to have zero PV at the surface and the level of the tropopause and explicit expressions for $G(z, z')$ are obtained easily (not shown). Writing $g_{ij} = G(z = i, z' = j)$ where $i, j = (0, d, h)$, we get for the CM with PV at level h (not residing at the steering level of the discrete NMs):

$$\frac{B}{Q} = \frac{\bar{q}_y^0\left[(c - c_T)g_{0h} - g_{0d}\bar{q}_y^d g_{dh}\right]}{(c - c_+)(c - c_-)}, \tag{B1}$$

$$\frac{T}{Q} = \frac{\bar{q}_y^d\left[(c - c_B)g_{dh} - g_{d0}\bar{q}_y^0 g_{0h}\right]}{(c - c_+)(c - c_-)}, \tag{B2}$$

where $c = \bar{u}(z = h)$ and $c_\pm$ are the solutions of the discrete NMs given in (9). Clearly these solutions become singular only for PV perturbations at the neutral branches of the discrete NM dispersion relation: If $c_\pm$ form a complex conjugate pair $c_\pm = \bar{c} \pm ic_i$, the denominator in the above equations becomes $(c - c_+)(c - c_-) = (c - \bar{c})^2 + c_i^2$ which is real and positive. On the other hand, if $c_\pm = \bar{c} \pm c_r$ we get $(c - c_+)(c - c_-) = (c - \bar{c})^2 - c_r^2$ which can (and does) become zero for $c = c_\pm = \bar{c} \pm c_r$.

References

Blumen, W. 1979. On short-wave baroclinic instability. *Journal of the Atmospheric Sciences*, **36**, 1925–1933.

Blumsack, S. L. and Gierasch, P. J. 1972. Mars: The effects of topography on baroclinic instability. *Journal of the Atmospheric Sciences*, **29**, 1081–1089.

Bordi, I., Dell'Aquila, A., Speranza, A. and Sutera, A. 2002. Formula for a baroclinic adjustment theory of climate. *Tellus*, **54A**, 260–272.

Bretherton, F. P. 1966. Baroclinic instability and the short wavelength cut-off in terms of potential vorticity. *Quarterly Journal of the Royal Meteorological Society*, **92**, 335–345.

Chang, E. K. M. 1992. Resonating neutral modes of the Eady model. *Journal of the Atmospheric Sciences*, **49**, 2452–2463.

Charney, J. G. and Stern, M. E. 1962. On the stability of internal baroclinic jets in a rotating atmosphere. *Journal of the Atmospheric Sciences*, **19**, 159–172.

Davies, H. C. and Bishop, C. H. 1994. Eady edge waves and rapid development. *Journal of the Atmospheric Sciences*, **51**, 1930–1946.

De Vries, H. and Opsteegh, J. D. 2005. Optimal perturbations in the Eady model: Resonance versus PV unshielding. *Journal of the Atmospheric Sciences*, **62**(2), 492–505.

De Vries, H. and Opsteegh, J. D. 2006. Dynamics of singular vectors in the semi-infinite Eady model: nonzero β but zero mean PV gradient. *Journal of the Atmospheric Sciences*, **63**2, 547–564.

Dirren, S. and Davies, H. C. 2004. Combined dynamics of boundary and interior perturbations in the Eady setting. *Journal of the Atmospheric Sciences*, **61**, 1549–1565.

Eady, E. T. 1949. Long waves and cyclone waves. *Tellus*, **1**, 33–52.

Farrell, B. F. 1982. The initial growth of disturbances in a baroclinic flow. *Journal of the Atmospheric Sciences*, **39**, 1663–1686.

Farrell, B. F. 1984. Modal and non-modal baroclinic waves. *Journal of the Atmospheric Sciences*, **41**, 668–673.

Gill, A. E. 1982. *Atmosphere-Ocean Dynamics*. Academic Press, Inc., pp. 662, 1st edition.

Heifetz, E. and Methven, J. 2005. Relating optimal growth to counter-propagating Rossby waves in shear instability. *Physics of Fluids*, **17**, 064107.

Heifetz, E., Bishop, C. H., Hoskins, B. J. and Methven, J. 2004a. The counter-propagating Rossby-wave perspective on baroclinic instability. I: Mathematical basis. *Quarterly Journal of the Royal Meteorological Society*, **130**, 211–231.

Heifetz, E., Methven, J., Hoskins, B. J. and Bishop, C. H. 2004b. The counter-propagating Rossby-wave perspective on baroclinic instability. II: Application to the Charney model. *Quarterly Journal of the Royal Meteorological Society*, **130**, 233–258.

Hoskins, B. J., McIntyre, M. E. and Robertson, A. W. 1985. On the use and significance of isentropic potential vorticity maps. *Quarterly Journal of the Royal Meteorological Society*, **111**, 877–946.

Jenkner, J. and Ehrendorfer, M. 2006. Resonant continuum modes in the Eady model with rigid lid. *Journal of the Atmospheric Sciences*, **63** 2, 765–773.

Juckes, M. N. 1994. Quasigeostrophic dynamics of the tropopause. *Journal of the Atmospheric Sciences*, **51**, 2756–2768.

Liu, Y. and Mu, M. 1996. Nonlinear stability theorem for Eady's model of quasigeostrophic baroclinic flow. *Journal of the Atmospheric Sciences*, **53**, 1459–1463.

Liu, Y. and Mu, M. 2001. Nonlinear stability of the generalized Eady model. *Journal of the Atmospheric Sciences*, **58**, 821–827.

Methven, J., Heifetz, E., Hoskins, B. J. and Bishop, C. H. 2005. The counter-propagating Rossby-wave perspective on baroclinic instability. III: Primitive-equation disturbances on the sphere. *Quarterly Journal of the Royal Meteorological Society*, **131**, 1393–1424.

Methven, J., Hoskins, B. J., Heifetz, E. and Bishop, C. H. 2005. The counter-propagating Rossby-wave perspective on baroclinic instability. IV: Nonlinear life cycles. *Quarterly Journal of the Royal Meteorological Society*, **131**, 1425–1440.

Morgan, M. C. and Chen, C. C. 2002. Diagnosis of optimal perturbation evolution in the Eady model. *Journal of the Atmospheric Sciences*, **59**, 169–185.

Mu, M. and Shepherd, T. G. 1994. Nonlinear stability of Eady's model. *Journal of the Atmospheric Sciences*, **51**, 3427–3436.

Müller, J. C. 1991. Baroclinic instability in a two-layer, vertically semi-infinite domain. *Tellus*, **43A**, 275–284.

Pedlosky, J. 1964. An initial value problem in the theory of baroclinic instability. *Tellus*, **16**, 12–17.

Pedlosky, J. 1987. *Geophysical Fluid Dynamics*. Prentice Hall, New Jersey, pp. 710, 2nd edition.

Ripa, P. 2001. Waves and resonance in free-boundary baroclinic instability. *Journal of Fluid Mechanics*, **428**, 387–408.

Rivest, C., Davis, C. A. and Farrell, B. F. 1992. Upper-tropospheric synoptic-scale waves. part I: Maintenance as Eady normal modes. *Journal of the Atmospheric Sciences*, **49**, 2108–2119.

Simmons, A. J. 1974. Baroclinic instability at the winter stratopause. *Quarterly Journal of the Royal Meteorological Society*, **100** 426, 531–540.

Song, Y. and Nakamura, N. 2000. Eady instability of isolated baroclinic jets with meridionally varying tropopause height. *Journal of the Atmospheric Sciences*, **57**, 46–65.

Thorncroft, C. D. and Hoskins, B. J. 1990. Frontal cyclogenesis. *Journal of the Atmospheric Sciences*, **47**, 2317–2336.

Weng, H. Y. and Barcilon, A. 1987. Favorable environments for explosive cyclogenesis in a modified two-layer Eady model. *Tellus*, **39A**, 202–214.